STATCOM Controller Design for Hybrid PV-Wind of AC Microgrid

Dawood Saleem Ahmed[*], Ali F. Marhoon[**]

[*]Training and Energy Research Office, Ministry of Electricity, Iraq
Email: Dawoodalameen41@gmail.com
https://orcid.org/0009-0002-5679-1430

[**]Electrical Engineering Department, College of Engineering, University of Basrah, Iraq
Email: ali.marhoon@uobasrah.edu.iq
https://orcid.org/0000-0003-0301-5200

Abstract

In recent years, Microgrid has become more attractive. A combination of renewable energy resources with load at the distribution level appears preferable. However, such a combination is challenging to work correctly. Power system indices such as voltage and frequency appear difficult to be within an allowable limit. This research will use a STATCOM compensator to increase the voltage stability of the power system containing wind and solar energy generation systems. The STATCOM based modular multi-level converter is designed to increase the output voltage quality and reduce filter requirements. The proportional and integral (PI) and integral sliding mode (ISM) controller is designed in a MATLAB/SIMULINK environment. The results demonstrate the effectiveness of the STATCOM compensator in this hybrid system with both PI and ISM controllers.

Keywords- — STATCOM, Microgrid, Wind Power, Photovoltaic.

I. INTRODUCTION

Recently, decentralized generators, such as renewable energy generators, have been integrated into the distribution network, establishing the Microgrid concept. Microgrids (MGs) are small-scale electrical grids that include linked loads and dispersed generation resources [1]. Researchers are exploring the possibility of integrating renewable energy sources (RESs) into the existing power grid as a reliable and secure option to tackle the problem of deteriorating generation, transmission, and distribution infrastructures [2]. In recent years, there has been a substantial surge in the utilization of RES in response to the growing energy demand, resulting in a rapid transition in energy production. This implies the need to research decentralized alternative energy and production. It is feasible to create a hybrid structure that combines a high-performing photovoltaic (PV) system with a wind energy system (WES) for applications that do not require significant power. Nevertheless, renewable energy solutions, such as wind power or a combination of wind and photovoltaics (PV), cannot provide absolute assurance in fulfilling the load requirement. Instability in power supply necessitates the inclusion of reactive power correction to prevent voltage fluctuations and ensure the stable operation of a hybrid system. As per IEEE Standard 1547.2-2008, it is required that both the manufacturer and the utility ensure that voltage variations do not exceed 5% and that voltage imbalance, defined by % imbalance or %VUF, falls within the range of 2.0% to 3.0%. Unbalance and VUF are quantified as the percentage of the greatest deviation from the average value and the ratio of the negative-sequence voltage to the positive-sequence voltage. Voltage breakdown has emerged as a critical concern in the electrical power system. This is due to its role as the primary catalyst for numerous significant power outages worldwide, including the notable incident in North America in August 2003 [8]. Inadequate provision of reactive power to the electricity grid during any unexpected situation can harm the system's stability, perhaps leading to a voltage collapse. The STATCOM offers advanced features such as the ability to control reactive power to mitigate voltage fluctuations, compensate for harmonic currents, mitigate voltage sags and flicker, compensate for neutral currents, and balance loads. Additionally, if the STATCOM is equipped with an energy storage system like a battery, it can participate in frequency regulation [3]. Consequently, numerous research studies suggest the use of STATCOM as a solution to address voltage fluctuations in MG [4]. The voltage at the Point of Common Coupling (PCC) exhibits substantial swings in response to load or active power requirement variations. Small wind power plants and solar power plants in MG experience inconsistent resource availability, which increases the electrical grid's vulnerability to stability issues. A wind power plant requires reactive power, specifically a Doubly Fed Induction Generator (DFIG). This reactive power is often obtained from the utility grid when it is accessible. The lack of a reactive power supply without the grid results in a low power factor. The research conducted in

reference [5] employs STATCOM to improve power factor and mitigate voltage issues in an MG. The work involved designing a STATCOM using two parallel six-pulse converters to generate a higher PWM output voltage. The MG in this study comprises two sources, namely hydropower plants and wind power plants, operating in an isolated network. Modelling MG can be highly complex due to factors such as line impedance and resistance that cannot be disregarded and the presence of inverters, which are typically encountered. However, these factors also make the modelling process more manageable. The fuzzy Proportional-Integral (PI) and fuzzy Proportional-Integral-Derivative (PID) controllers were used to regulate the STATCOM and evaluate its performance compared to conventional PI control. The outcome demonstrates superior power quality performance when utilizing a fuzzy controller. The study in [6] examined the interaction between STATCOM and various voltage source inverters in an isolated MG. This investigation utilized the impedance model and Nyquist stability criterion. The research has demonstrated that both the battery power converter and STATCOM exhibited instability. To address this issue, it is recommended to modify the impedance of the STATCOM using a lead-lag compensator. Nevertheless, the phase locked loop (PLL) dynamic was omitted in this study. In MG; inverters are essential for transferring power from resources to the load. Recently, multilevel inverters have gained more attention due to high quality output voltage waveform this merit means minimum harmonic therefore reduce filters requirements can be obtained. Among multilevel inverter the modular multilevel inverter (MMC) is used in this study due to its constricted that allows obtaining higher voltage levels and suitable for higher power applications [7]. There are four types of MMC: single star bridge cell, single delta bridge cell, double star chopper cell, and double star bridge cell [8]. This converter is first introduced by [9]. However, researchers have addressed some difficulties in designing this type of converter, such as circulating current among their phases and capacitor voltage balancing. Therefore, in the publication [10], the author suggests a circulating current suppression control scheme for MMC_STATCOM to address negative sequence compensation resulting from an unbalanced load. Nevertheless, the controller was designed based on the assumption that the grid utility is accessible and rigid, which is not the case in the distribution system or the MG. In [10] battery based energy storage system is added to the STATCOM to avoid power fluctuation caused by the wind power variation. In MMC converter DC capacitors, balance is an important aspect; therefore, in [11], an energy balancing control is proposed in order not only for the capacitor's DC voltage balance but also for total system stability. Hardware design and implementation of the MMC converter family require knowing some factors related to each type of these converters [12]. The comparison between MMC converter family is made in order to simplify the design procedure. The STATCOM in this study was modeled by an MMC converter in order to exploit the merits of this type of converter. This paper proposes an enhancement to address the unsatisfactory performance of the proportional-integral (PI) controller caused by uncertainties in system parameters and capacitors voltage control efforts using optimally PI and ISM controller.

II. MICROGRID SYSTEM MODEL

Hybrid solar photovoltaic (PV) and wind production systems have gained significant appeal, especially for independent applications. The integration of solar and wind energy sources enhances reliability. It improves the economic efficiency of the hybrid system by using the strengths of each source to compensate for the weaknesses of the other. Integrating hybrid solar and wind power systems into the grid can enhance the overall economy and the dependability of renewable power generation to meet its load. MG in this study consists of a wind energy conversion system (WECS), photovoltaic system (PV), and STATCOM. Modelling allows an understanding of the system's behavior under all disturbances and in steady-state conditions; therefore, the brief model used in this study will be introduced in the next section.

A. Photovoltaic PV System Model

Solar photovoltaic (PV) panels convert solar energy into direct current (DC) electricity. Several solar cells are connected in series or parallel and mounted on a surface to form a solar cell module, also known as a photovoltaic module, to increase power production. The one-diode equivalent circuit represents the photovoltaic (PV) cells, and the current generated by the PV cells may be calculated using the equation provided by [13][14].

$$I = I_{ph} - I_0 \left[e^{(V+IR_s)*\frac{q}{nkTN_s}} - 1 \right] - \frac{V+IR_s}{R_{sh}} \qquad (1)$$

Where: I_{ph} is the current generated due to the light, k is the Boltzmann gas constant and equals to (1.38*10^(-23) J/K), q is the electron charge and is equal to (1.6*10^(-19) C), T is the absolute temperature in Kelvin, n is linearity factor, N_s is the number of series PV modules, R_{sh} is the cell series resistance, V is the output voltage of the solar cell, and I_0 is the dark saturation current. The mathematical model of the photovoltaic system, as described in the previous section, is implemented in Simulink. Furthermore, the perturbation and observation (P&O) technique has been utilized to implement maximum power point tracking (MPPT) in photovoltaic (PV) power systems [15]. An inherent limitation of using a PV system is that when it is connected to the utility network, there is typically an increase in voltage at the point of standard coupling (PCC). As a result, numerous utilities develop their own guidelines, although the fundamental limitations are usually the same.

B. Wind energy conversion system (WECS)

WECS converts the kinetic energy of wind into electrical power. Basically, there are two types of wind turbine vertical axis and horizontal axis, the maximum power P_{wind} extracted from the wind by WTG is given as [16].

$$P_{wind} = \frac{1}{2}\rho\pi R^2 V^3 \quad (2)$$

Where; P_{wind}, ρ, R, and V are the wind power available, air density that is givn in (kg/m^2), the radius of the turbine blade in meters, and the wind speed in (m/s).

$$P_m = \frac{1}{2}\rho A {U_w}^3 C_P(\lambda,\beta) \quad (3)$$

$$C_P = 0.73\left[\frac{151}{\lambda_i} - 0.58\beta - 0.002\beta^{2.14} - 13.2\right]e^{\frac{-18.4}{\lambda_i}} \quad (4)$$

With

$$\lambda = \frac{\omega_{rot} r}{V_w} \quad and \quad \frac{1}{\lambda_i} = \frac{1}{\lambda - 0.02\beta} - \frac{0.003}{\beta^3 + 1} \quad (5)$$

Where A = rotor swept area, V_w = wind speed, C_P= power coefficient, λ= tip speed ratio, β = pitch angle. The relation between C_P and λ at various β is given in Fig.1.
The mechanical torque (Tm) developed in wind power can be expressed as in equation below:

$$T_m = \frac{P_m}{\omega_t} = \frac{0.5 C_p(\lambda,\beta)\rho\pi r^2 v^3}{\omega_t} \quad (6)$$

Where ω_t is turbine speed.

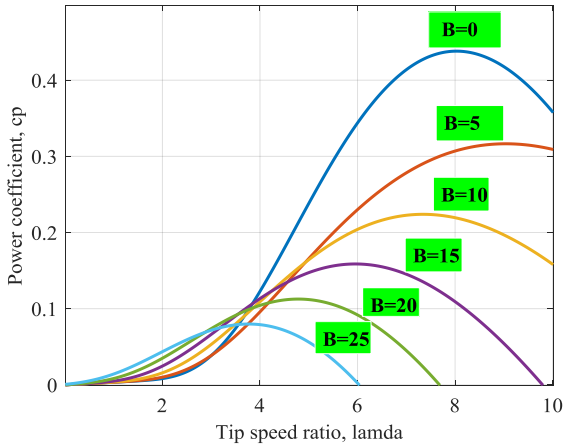

Figure 1. The relationship between power coefficient and tip speed ratio at various angles beta.

Wind turbine generators (WTG) are classified into two main types: fixed and variable speed machines. Variable speed is more efficient than fixed speed. Fixed speed WTG uses cage induction generator types which are directly connected to the network through a transformer. For a wide speed control range, a doubly fed induction generator (DFIG) is used with a partial back-to-back converter, as shown in Fig.2.

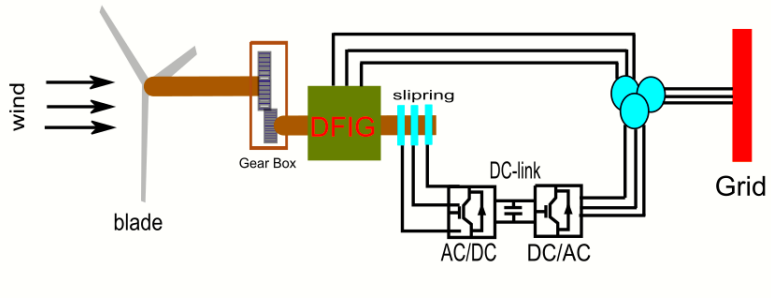

Figure 1. A DFIG based WTG.

Fig. 3 shows the mechanical system that two mass shift systems can model. The derivative of the mathematical description of the mechanical and electrical system can be found in [17] [18][14].

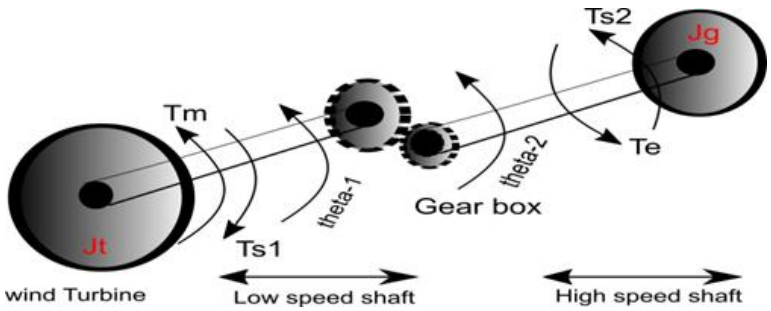

Figure 2. TWO MASS MODEL OF THE MECHANICAL SHAFT SYSTEM.

The control algorithm in the DFIG to cope with variable wind speed can be achieved by partial power grid side and rotor side converters. The grid side converter connected to the fixed frequency utility grid maintains the DC link voltage and can be used to maintain the power factor at the connection point with a grid. The rotor side converter is a frequency converter that produce variable voltage with variable frequency as required to ensure successful energy transfer between rotor and stator this can be accomplished by controlling rotor currents. This study exploited the control algorithm based stationary reference frame to implement indirect speed control. The DFIG data in Table 1 is used with characteristics as shown in Fig.4 (A) to produce a speed-power relation.

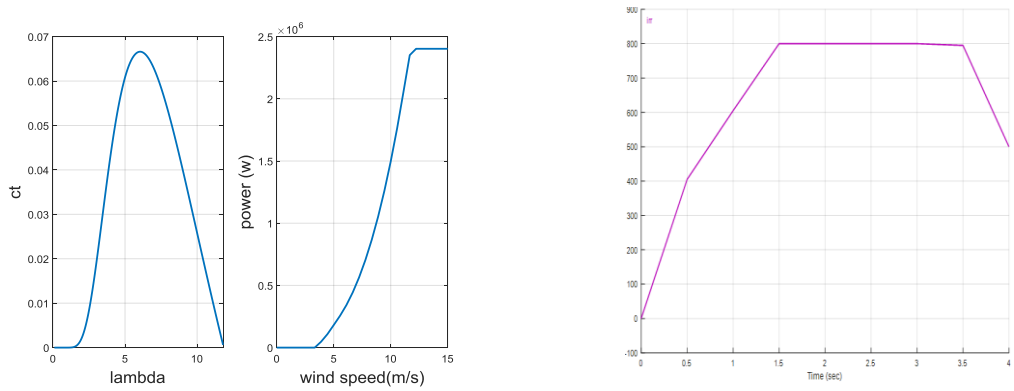

(A) (B)

Figure 3. (a) double fed induction generator wind speed Characteristics, (b) photovoltaic Characteristics.

C. Design and Modeling of STATCOM Controller

This section presents the Modeling of STATCOM used to model PI and integral sliding mode control strategies. The integral sliding mode control (ISMC) design for STATCOM is also presented in this section in order to compare the results for both controllers. The mathematical model with an equivalent circuit is required to design the PI and ISM controls strategy and analyze the dynamic response with characteristics of the STATCOM. Fig.5 shows the equivalent circuit of the STATCOM [19] and can be described by the following differential equations:

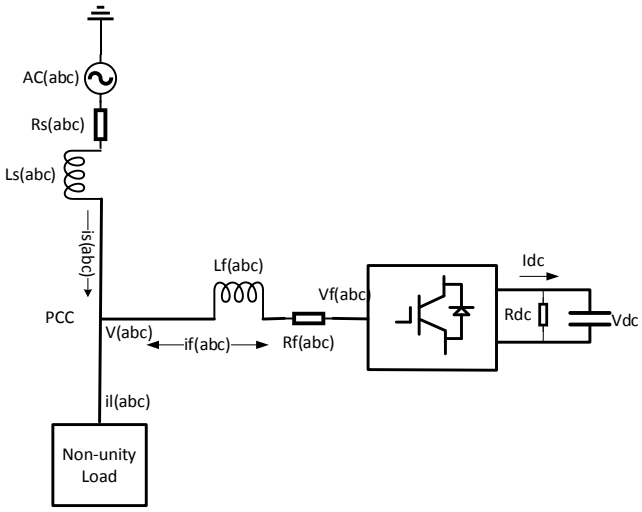

Figure 4. Equivalent Circuit of the STATCOM.

$$L_f \frac{di_{fa}}{dt} + R_f i_{fa} = v_a - v_{fa}$$

$$L_f \frac{di_{fb}}{dt} + R_f i_{fb} = v_b - v_{fb} \quad (7)$$

$$L_f \frac{di_{fc}}{dt} + R_f i_{fc} = v_c - v_{fc}$$

$$C \frac{d_{vdc}}{dt} + \frac{V_{dc}}{R_{dc}} = i_{dc} \quad (8)$$

To convert the system equations to the dq frame the following transformation matrix is used:

$$[T] = \sqrt{\frac{2}{3}} \begin{bmatrix} \cos(\theta) & \cos\left(\theta - \frac{2\pi}{3}\right) & \cos\left(\theta + \frac{2\pi}{3}\right) \\ -\sin(\theta) & -\sin\left(\theta - \frac{2\pi}{3}\right) & -\sin\left(\theta + \frac{2\pi}{3}\right) \\ \frac{1}{\sqrt{2}} & \frac{1}{\sqrt{2}} & \frac{1}{\sqrt{2}} \end{bmatrix} \quad (9)$$

The dq voltage and current can be determined as bellow:

$$[f_{dq}] = [T][f_{abc}] \quad (10)$$

Where:

T is the transformation matrix, f_{dq} represents the dq components of the abc phases of the voltage and current. The mathematical model of the STATCOM is mentioned in many references, such as [20]. In this study, the equation that will be used to describe the final STATCOM model is given in dq synchronous reference frame by substitution Equations (7, 8, and 9) into Equation (10) as follows:

$$\frac{di_{fd}}{dt} = -\frac{R_f}{L_f} i_{fd} + \omega i_{fq} + \frac{v_{fd} - v_d}{L_f}$$

$$\frac{di_{fq}}{dt} = -\frac{Rr}{L_f} i_{fq} - \omega i_{fd} + \frac{v_{fq}}{L_f} \qquad (11)$$

$$\frac{dV_{dc}}{dt} = \frac{1}{C}(i_{dc}) - \frac{1}{CR_{dc}} V_{dc}$$

Where: i_{fd}, and i_{fq} are d, and q components of STATCOM current respectively. V_{dc} is the STATCOM DC-link bus voltage. i_{dc} is the input DC current of the STATCOM inverter. C is DC-link capacitor, and the resistance R_{dc} represents the switching losses estimation. This model will be used for designing both PI and the integral sliding mode controller of the system PCC voltage control and V_{dc} voltage control. PI control is commonly employed in industrial control systems because parameters about the system's output characteristics can be adjusted. The following is a general Equation of the PI controller and adopted here for the STATCOM equations [21]:

$$i_{fdqref}(t) = K_p e_{1,2}(t) + K_i \int e_{1,2}(t)dt \qquad (12)$$

Where:

$e(t)_1 = V_{dcref}(t) - V_{dc}(t)$ and $e(t)_2 = V_{ref}(t) - V(t)$

Where $i_{f_{dqref}}$ are the output of the two voltage controllers, e(t) represents the error signal between the desired (V_{pcc} and V_{dc}) and its measured quantities, $K_p$and K_i are the proportional and integral gains of the PI controller, respectively. The $i_{f_{dqref}}$ then compare with measured values; the error signal then passes through another PIs current controller to produce the modulated signal $u_{d,q}$ (t) as given in Equation (13).

$$u_{d,q}(t) = K_p e_{3,4}(t) + K_i \int e_{3,4}(t)dt \qquad (13)$$

Where:

$e_3(t) = i_{fdref}(t) - i_{fd}(t)$ and $e_4(t) = i_{fqref}(t) - i_{fq}(t)$. The implementation of the above method is shown in Fig. 6.

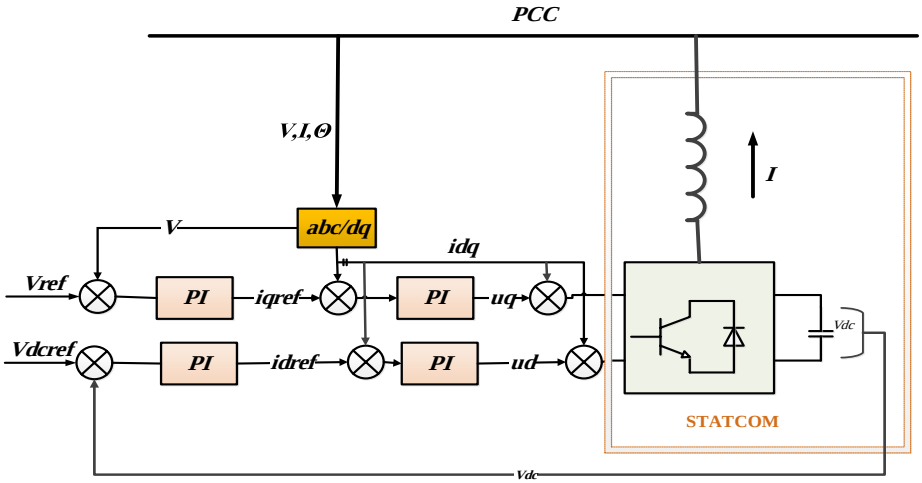

Figure 5. PI based Controller

SMCs are used to control PCC and V_{dc} voltages. The first step in designing the SMC is to form the sliding surface. In general, the equation primarily used for the sliding surface can be written in terms of error as follows:

$$s(t) = C\,e(t) + \dot{e}(t) \qquad (14)$$

$$\dot{s}(t) = C\,\dot{e}(t) + \ddot{e}(t) \qquad (15)$$

Where C is a positive constant in both above equations. It is shown that sliding surface is an action related to tracking error, which is any difference between reference and actual output. C > 0 is a performance parameter that guarantees the system's stability on the sliding surface in addition, the sliding function and its derivative over the sliding surface are both equal to zero such that $s(t)$ and $\dot{s}(t) = 0$.

The ISMC has been chosen to be used in this study to control the MMC-STATCOM in the hybrid environment PV/Wind specifically to regulate PCC and V_{dc} voltages. In this case, the objective is to regulate V_{pcc} to V_{pccref} and also to regulate the V_{dc} to follow V_{dcref}. The integral sliding surface for the system is given below:

$$S_{vpcc} = k_{pvpcc}(v_{pcc} - v_{pccref}) + k_{ivpcc}\int (v_{pcc} - v_{pccref})dt \qquad (16)$$

Control law of this controller is given by

$$i_{fqref} = -k_{vpcc}\,\mathrm{sign}(S_{vpcc}) \qquad (17)$$

Where: all the gains in above equations are positive numbers. The chattering phenomenon effect is the most known drawback of using the integral SMC. Generally, this problem is due to the discontinuous control action with an ideal infinite frequency. Numerous solutions are proposed to avoid undesirable chattering. The most common solution is to use continuous switching functions instead of discontinuous ones. This study will use smooth function in the integral SMC instead of the sign function. In order to regulate V_{dc} , the integral sliding surface can be given as follows:

$$S_{dc} = k_{pdc}(v_{dc} - v_{dcref}) + k_{idc}\int (v_{dc} - v_{dcref})dt \qquad (18)$$

The equivalent control can be calculated from $\dot{s} = 0$, and the stabilizing control is given to ensure the convergence condition. Hence, the following control law can be deduced:

$$v_{dc} = \frac{1}{g_{vdc(x)}}\left(\left(-f_{vdc}(x) + \frac{d_{vdcref}}{dt}\right) - \frac{k_{idc}}{k_{pdc}}(v_{dc} - v_{dcref})\right) - k_{dc}\,\mathrm{sign}(S_{dc}) \qquad (19)$$

Where: k_{idc}, k_{pdc} and k_{dc} are positive constants. The implementation of this method is shown in Fig.7.

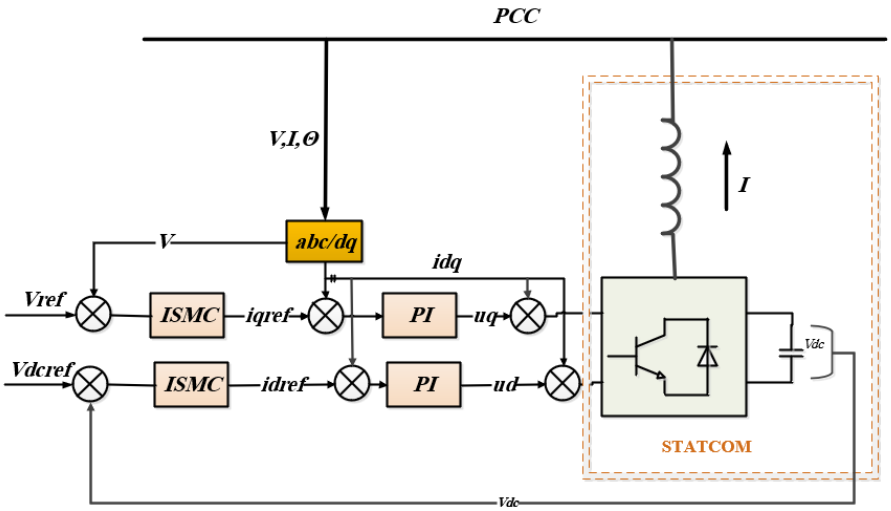

Figure 6. ISMC based Controller

III. CASE STUDY AND RESULTS

MATLAB/Simulink is used to model the microgrid system, which consists of variable wind power conversion and photovoltaic systems in isolation mode. The wind power conversion system is represented by a doubly fed induction generator with a rated capacity equal to 2MW. This system can be controlled in two different modes: maximum power point tracking (MPPT), which is used if the wind speed available is not sufficient, whereas when the wind speed is at rated speed, the control is changed to speed control. However, in this study, only MPPT represents the worst case, as wind speed is about 8.5 m/s, as shown in Figure 3 (A) above. Another renewable resource is a PV system with a rated capacity of 100 kW. The configuration of the PV system is the two stage configurations; a boost converter first boosts the DC voltage and then converted to AC by a dedicated inverter. MPPT controls the boost converter to track the sun irradiance curve as shown in Figure 3 (B). The system load is modelled as a balanced three phase aggregated load with 4.5MW and 0.5MVAR. The diesel generation system is assumed to be 2.4kV 3MW with a step up transformer 2.4/11kV 3.5MVA [22]. The block diagram of the MG system is first introduced, as shown in Figure 8, and the rest of the system data are given in the appendix.

- STEADY STATE PERFORMANCE OF THE CASE STUDY

  In this case, the MATLAB/ SIMULINK is run without disturbance for four seconds, and the results of the electrical distribution system containing wind/PV and diesel power generation are shown in the Figures as follows:

ISSN: 2710-2165

Fig 9 and Fig10 show the more important factors related to wind power generation, Figure 11 and Figure 12 show the more important factors related to PV power generation.

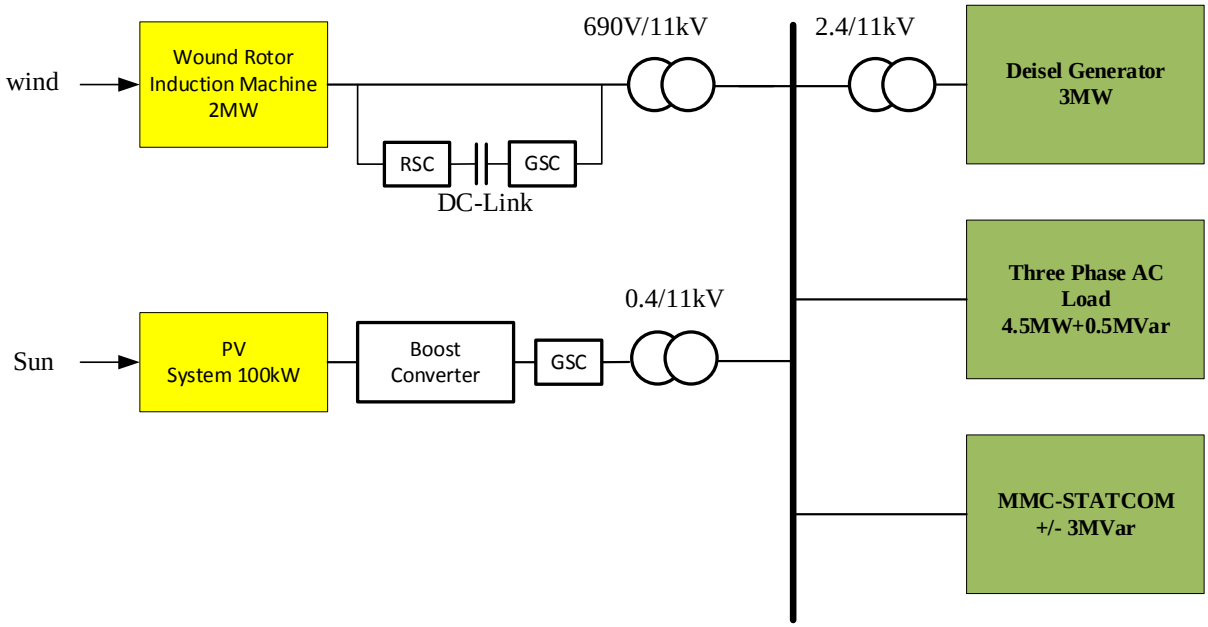

Figure 7. electrical distribution system under study

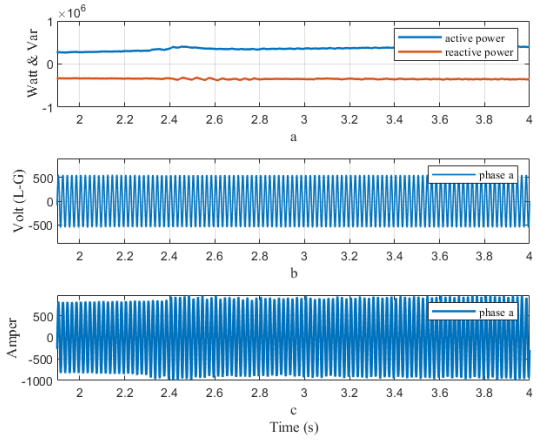

Figure 8. steady state performance of wind power generation, (a) stator active and reactive power, (b) stator voltage, (c) stator current.

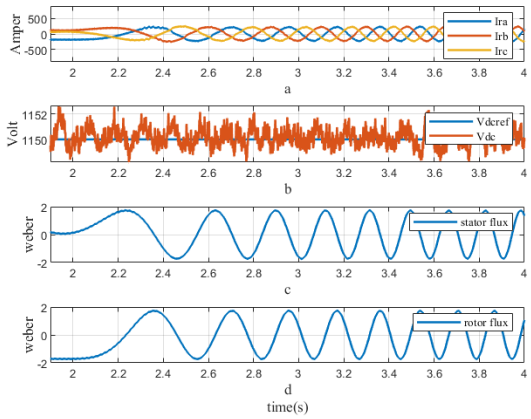

Figure 9. steady state performance of wind power generation, (a) rotor current, (b) dc link voltage of back to back converters, (c) stator flux, (d) rotor flux.

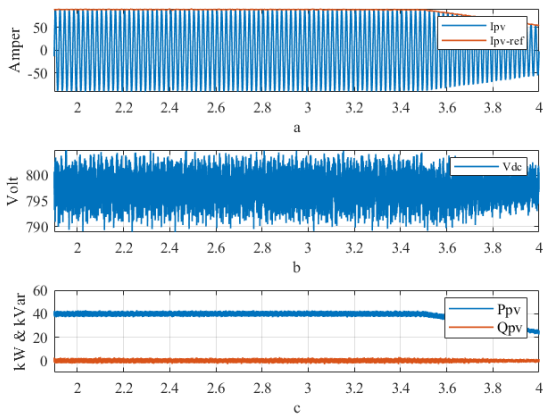

Figure 10. steady state performance of photovoltaic power generation, (a) tracking performance of pv current, (b) dc input power of pv inverter, (c) active and reactive power.

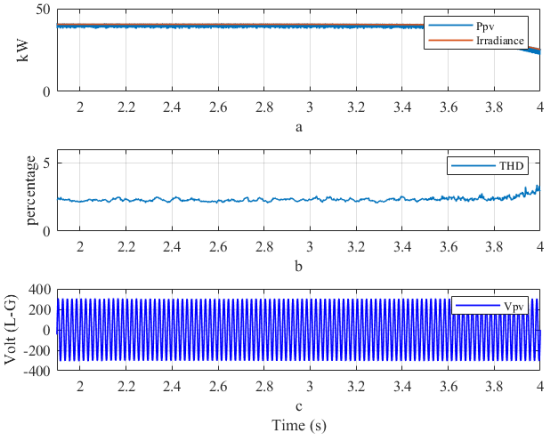

Figure 11. steady state performance of photovoltaic power generation, (a) tracking performance of pv power, (b) total harmonic distortion at pv bus, (c) inverter output voltage.

- PERFORMANCE DURING DISTRIBANCE OF THE CASE STUDY

  In this case, the electrical distribution system is imposed to the sag and swell disturbance. The disturbances are programmed as follows: Voltage dip occurs during time space 0.5 seconds from 2 to 2.5 seconds. Voltage swell occurs during time space 0.5 seconds from 3 to 3.5 seconds. It is worth noting that the STATCOM is not included in this case. Figures 13 and 14 show the wind power generation performance in case of the voltage dip and voltage swell occurrence. Figures 15 and 16 show the PV power generation system performance.

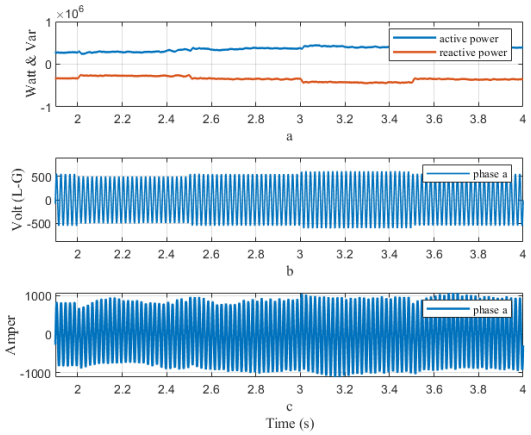

Figure 12. performance of wind power generation during disturbance, (A) stator active and reactive power, (B) stator voltage, (C) stator current.

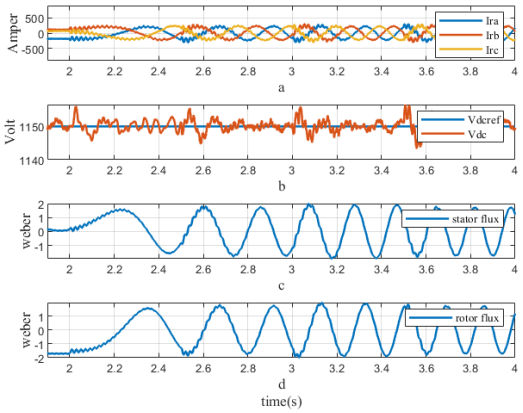

Figure 13. performance of wind power generation during disturbance, (a) rotor current, (b) dc link voltage of back to back converters, (c) stator flux, (d) rotor flux.

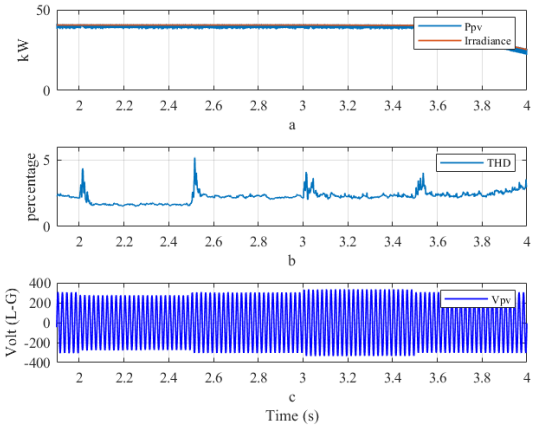

Figure 14. performance of pv power generation during disturbance, (a) tracking performance of pv current, (b) dc input power of pv inverter, (c) active and reactive power.

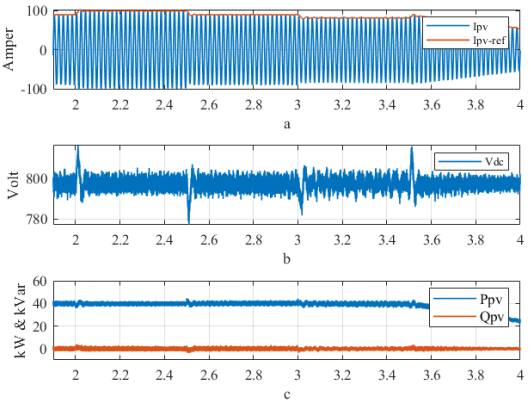

Figure 15. performance of pv power generation during disturbance, (a) tracking performance of pv power, (b) total harmonic distortion at pv bus, (c) inverter output voltage.

- PERFORMANCE DURING DISTURBANCE OF THE CASE STUDY WITH STATCOM

In this case, the STATCOM is included to inject or absorb the reactive power needed by the electrical system, especially during system disturbance. This is shown through the Figures (17, 18, 19, and 20). The reactive power absorbed by the wind power generation is nearly reduced due to STATCOM operation. In other words, the wind power generation system draws less current through the rotor side converter compared with the previous case when the STATCOM was not included. It is worth mentioning at this point that the electrical system performance is similar whether the STATCOM is controlled using PI or using ISMC. Therefore, the attention is now paid to the performance of the STATCOM controller in the electronic part.

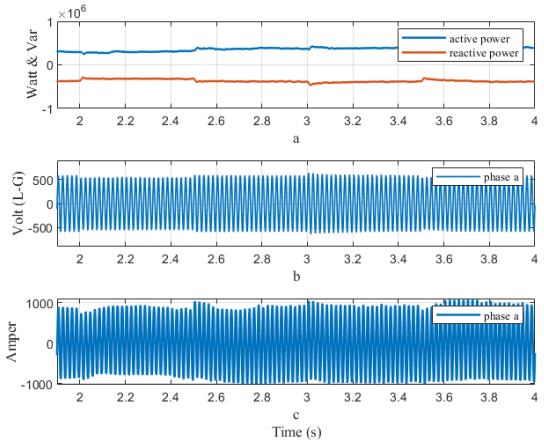

Figure 16. performance of wind power generation during disturbance with STATCOM, (A) stator active and reactive power, (B) stator voltage, (C) stator current.

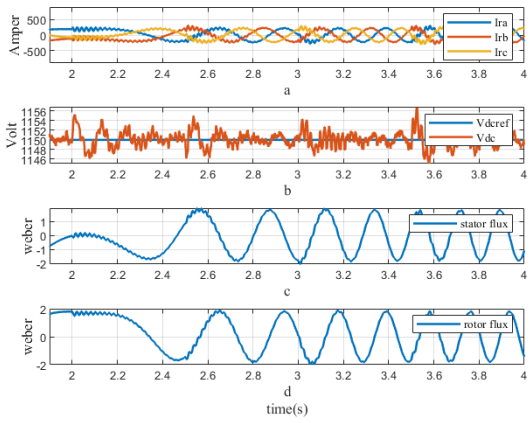

Figure 17. performance of wind power generation during disturbance with statcom, (a) rotor current, (b) dc link voltage of back to back converters, (c) stator flux, (d) rotor flux.

ISSN: 2710-2165

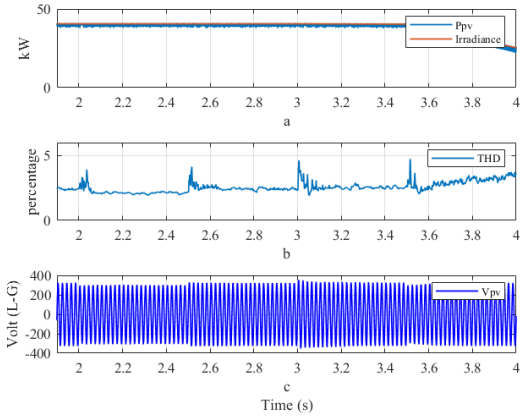

Figure 18. performance of pv power generation during disturbance with STATCOM, (a) tracking performance of pv current, (b) dc input power of pv inverter, (c) active and reactive power.

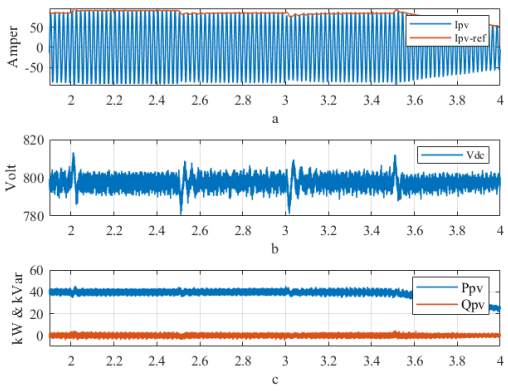

Figure 19. performance of pv power generation during disturbance with STATCOM, (a) tracking performance of pv power, (b) total harmonic distortion at pv bus, (c) inverter output voltage.

The STATCOM inverter shown in Fig.21 consists of eight capacitors in each arm that need to be charged and discharged in a harmonical manner; this can be done through capacitors voltage balancing control, hence avoiding the unbalance inside STATCOM converter and keeping reasonable circulating current among converter legs. In this study, a sorting algorithm is used to satisfy the capacitors balancing requirements. In addition, a level shift modulation scheme is adopted in this study to obtain the gates signal require to operate each power transistors this process is explained in Fig.22 [23].

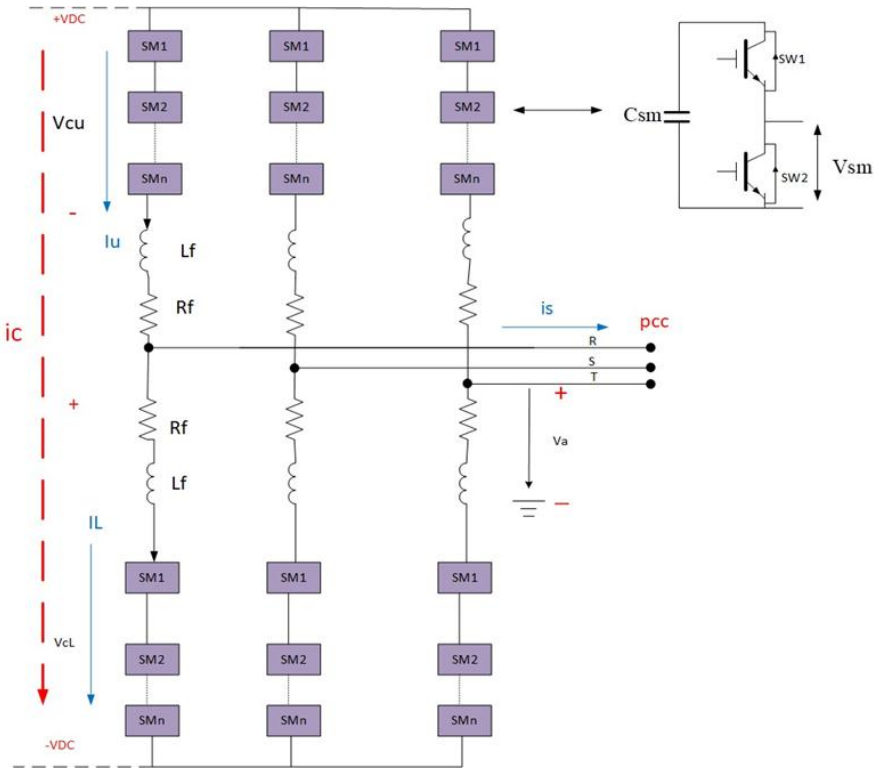

Figure 20. MODULAR MULTILEVEL CONVERTER DSCC TYPE.

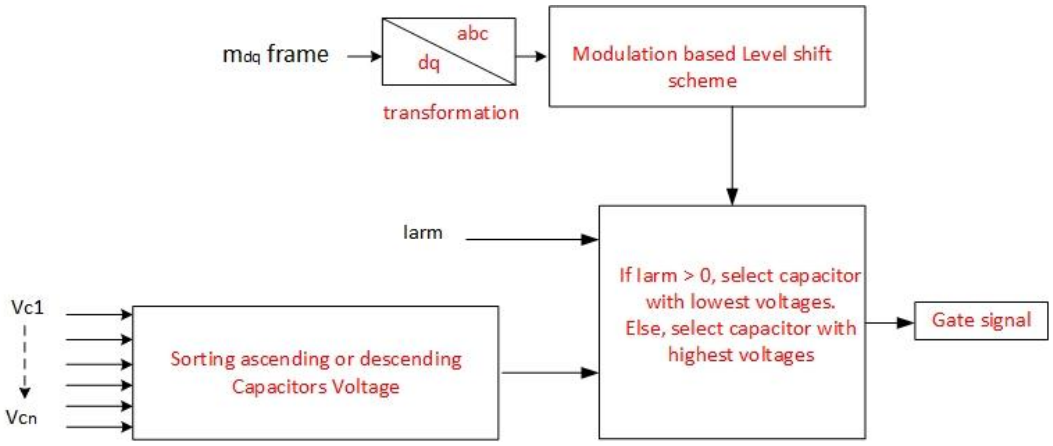

Figure 21. sorting algorithm procedure.

The performance of the STATCOM controller using conventional PI control is shown in the following figures. The capacitors voltages balancing is shown in Fig.23(a), the capacitors voltages reach a steady state within 0.5 seconds and start to follow the set point, which is 1400V; the overshoot is also observed in this figure. Fig23(b) displays the performance of the quadrature current control; the highlighted portions in this figure indicate that there are small swing in the reference tracking performance that led to more control action effort. Fig.24(a) shows the line-to-line output voltage of the STATCOM; this output voltage is nearly sinusoidal, leading to a few filter requirements. Fig.24(b) shows the average voltage of the DC capacitors voltages. This figure shows that there is a small swing when the disturbance occurs. Fig24(c) shows the STATCOM output voltage and current; the current behavior during disturbance is shown in the highlighted portion of this figure, where the current changes its sign from capacitive to inductive during disturbance. Fig.24(d) shows the STATCOM active and reactive power; it is worth mentioning the active power exchange with the electrical grid is zero as long as there is no energy source in the DC input port; therefore, only reactive power is export or import with the electrical grid is observed. Fig .25 (a) shows the upper and lower inverter current; during dip disturbance, an increase in this current is observed, and it decreases during voltage swell. The modulator produces eight levels for each converter arm, as shown in Fig. 25(b). The performance of the outer AC voltage and DC voltage controllers are shown in Fig 25 (c and d), respectively.

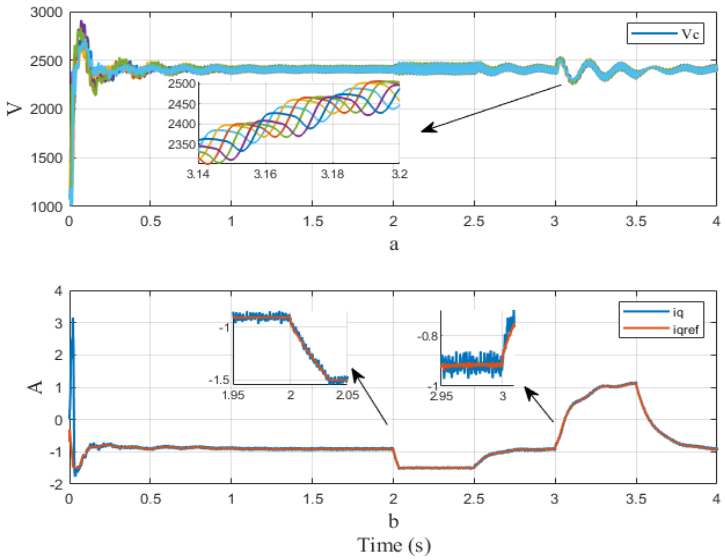

Figure 22. STATCOM controller performance, (a) capacitors voltages, (b) quadrature current tracking.

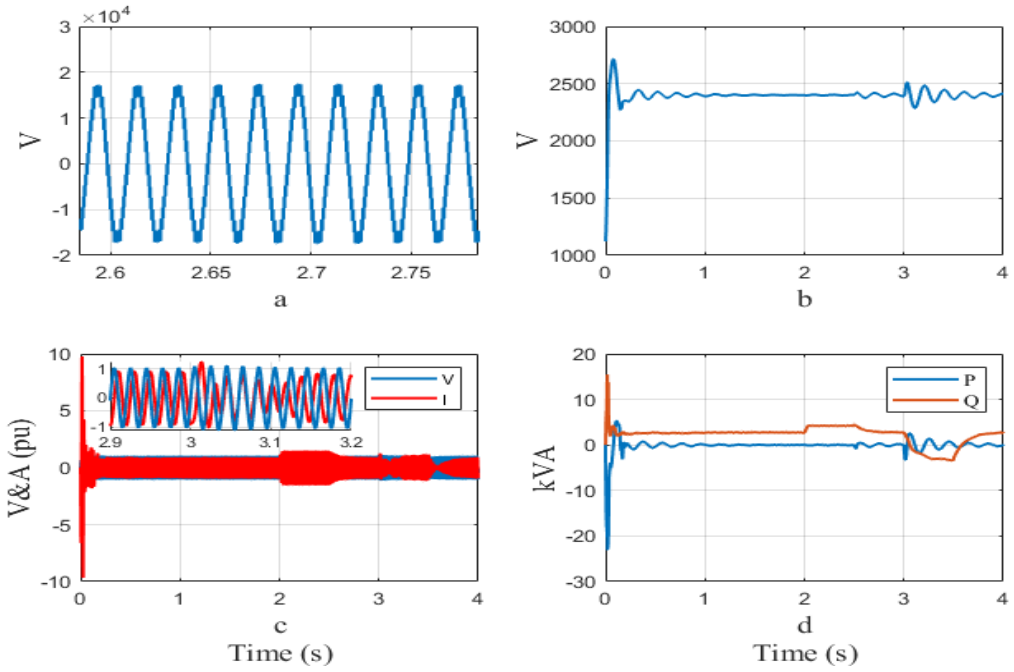

Figure 23. (a) STATCOM output voltage l-l, (b) STATCOM average dc link voltage, (c) STATCOM output voltage and current p.u, (d) STATCOM active and reactive power.

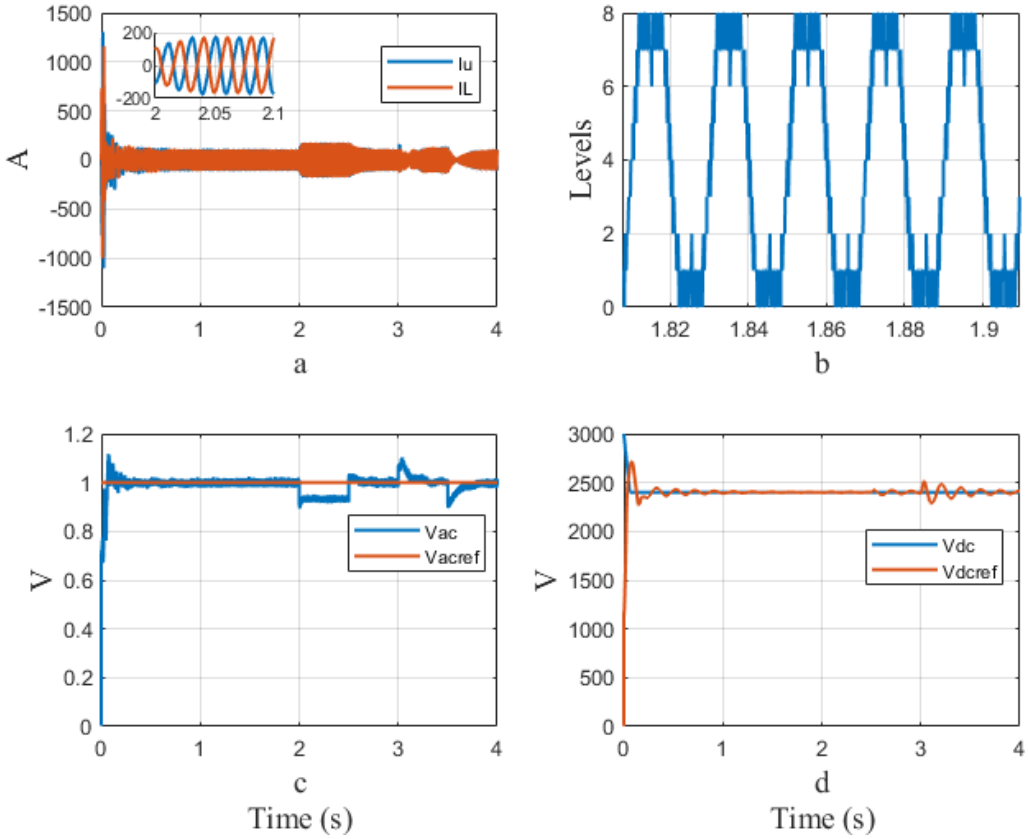

Figure 24. (a) STATCOM upper and lower arm current, (b) modulated signal, (c) ac voltage control performance, (d) dc voltage control performance.

The performance of the STATCOM controller using conventional ISM control is shown in the following figures. Compared with the previous case, the capacitors voltages balancing is shown in Fig.26 (a); the enhancement in the performance is clearly observed in

this figure, which shows a slight overshoot and faster reaching to the steady state. Fig. 26 (b) displays the performance of the current quadrature control, and the highlighted portions in this figure indicate that the tracking performance is better than that of the previous case. Fig. 27 (a) shows the line-to-line output voltage with good quality, similar to the previous case. Comparing Fig. 27 (b) with the previous case, one can observe no swing during system disturbance with good tracking performance. Fig. 27 (c) shows the STATCOM output voltage and current; the current behavior during disturbance is shown in the highlighted portion of this figure, where the current changes its sign from capacitive to inductive during disturbance. Fig.27 (d) shows the STATCOM active and reactive power; it is worth mentioning that the active power exchange with the electrical grid is zero as long as there is no energy source in the DC input port; therefore, only reactive power is export or import with the electrical grid is observed. Fig .28 (a) shows upper and lower inverter currents; during dip disturbance, an increase in this current is observed, and it decreases during voltage swell. The modulator produces eight levels for each converter arm, as shown in Fig. 28 (b). the performance of the outer AC voltage and DC voltage controllers are shown in Fig. 28 (c and d), respectively.

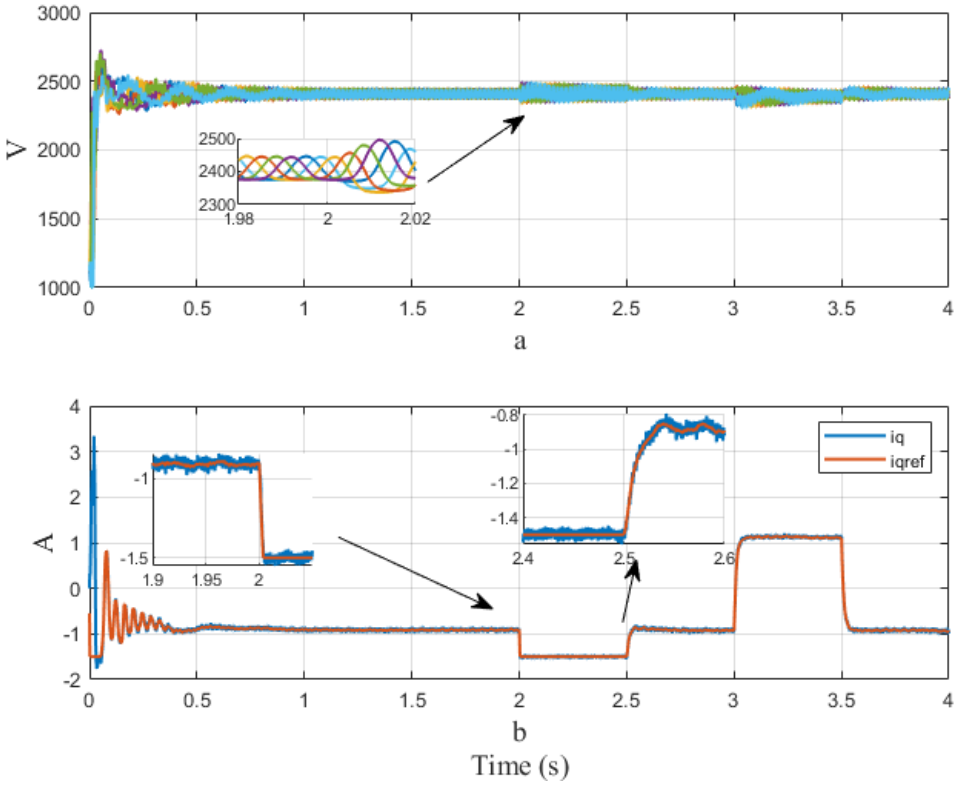

Figure 25. STATCOM controller performance, (a) capacitors voltages, (b) quadrature current tracking.

ISSN: 2710-2165

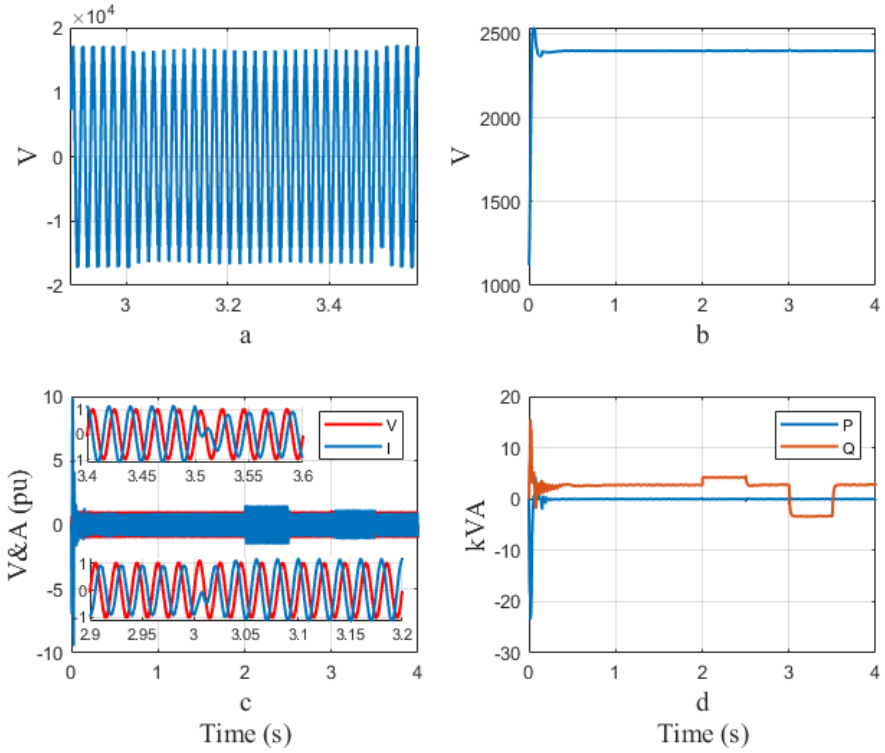

Figure 26. (a) STATCOM output voltage l-l, (b) STATCOM average dc link voltage, (c) STATCOM output voltage and current p.u, (d) STATCOM active and reactive power.

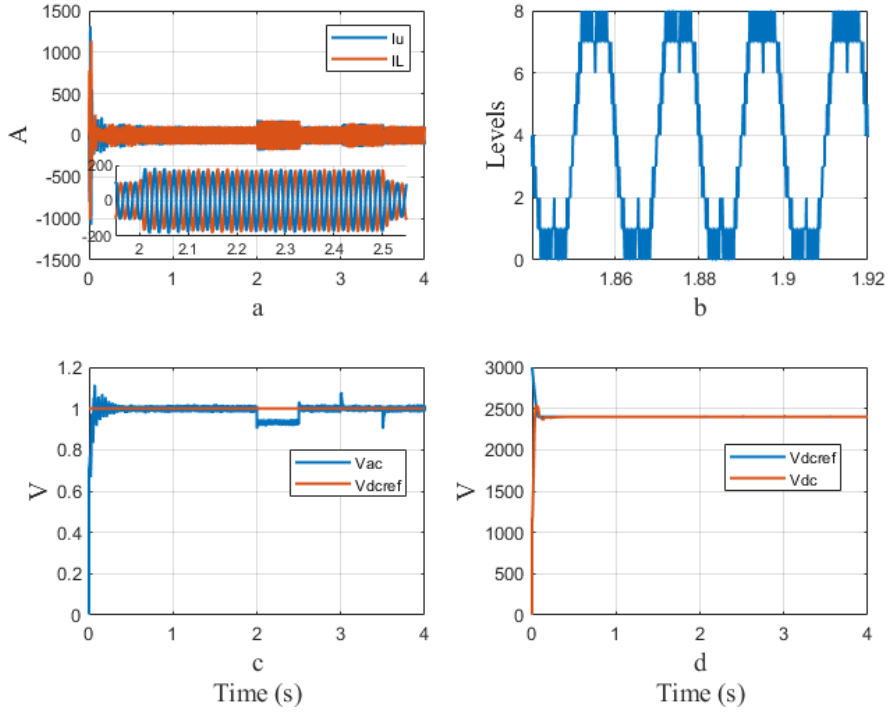

Figure 27. (a) STATCOM upper and lower arm current, (b) modulated signal, (c) AC voltage control performance, (d) DC voltage control performance.

IV. CONCLUSIONS

This research paper explains the hybrid PV/wind Microgrid AC electrical system model. In addition, the STATCOM controller is used to compensate for the reactive power during voltage sag and swell. Two types of controllers were used to drive the STATCOM controller: PI and ISM. MATLAB/SIMULINK is used to model the electrical system, including STATCOM. The STATCOM with ISMC in AC voltage and DC voltage controllers showed more remoteness against system disturbances.

V. APPENDIX

Table I system parameters

Parameters	Value	Features
Speed	*1500 rev/min*	Synchronous speed at 50 Hz
Rated power	*2 MW*	Nominal stator three-phase active power
Rated stator voltage	*690 Vrms*	Line-to-line nominal stator voltage in rms
Rated stator current	*1760 Arms*	Each phase nominal stator current in rms
Rated torque	*12.7 k.Nm*	Nominal torque at generator modes
p	*2*	Pair of poles
Rated rotor voltage	*2070 Vrms*	Line-to-line nominal rotor voltage in rms
Stator connection	*Star*	
Rotor connection	*Star*	
u	*0.34*	
R_s	*2.6 mΩ*	Stator resistance
$L_{\sigma s}$	*87 mH*	Stator leakage inductance
L_m	*2.5 mH*	Magnetizing inductance
R'_r	*26.1 mΩ*	Rotor resistance
$L'_{\sigma r}$	*783 mH*	Rotor leakage inductance
R_r	*2.9 mΩ*	Rotor resistance referred to the stator
$L_{\sigma r}$	*87 mH*	Rotor leakage inductance referred to the stator
L_s	*2.587 mH*	Stator inductance: $L_s = L_m + L_{\sigma s}$
L_r	*2.587 mH*	$L_r = L_r + L_{\sigma r}$
Csm	*5mH*	
Rarm	*0.065 ohm*	
Larm	*15mH*	
No.of submodel per arm	*8*	

Table 1 STATCOM controller parameters

Techniques	ISMC Controller gain	PI AC Voltage controller gains		PI DC Voltage controller gains		PI Quadrature current controller gains	PI direct current controller gains
	K	K_p	K_i	K_p	K_i	K_p	K_i
PI	-	0.55	2500	0.001	0.15	0.8	200
ISMC	0.1	0.5	2	0.11	0.56	0.6	150

REFERENCES

[1] P. Coelho, M. Gomes, and C. Moreira, *Microgrids Design and Implementation*. 2018. doi: 10.1007/978-3-319-98687-6_4.

[2] A. Ghosh and F. Zare, *Control of Power Electronic Converters with Microgrid Applications*. New Jersey: John Wiley & Sons, Inc., 2023.

[3] F. H. Gandoman *et al.*, "Review of FACTS technologies and applications for power quality in smart grids with renewable energy systems," 2018. doi: 10.1016/j.rser.2017.09.062.

[4] M. Ahmadi, P. Sharafi, M. H. Mousavi, and F. Veysi, "Power quality improvement in microgrids using statcom under unbalanced voltage conditions," *Int. J. Eng. Trans. C Asp.*, vol. 34, no. 6, pp. 1455–1467, 2021, doi: 10.5829/ije.2021.34.06c.09.

[5] M. M. Hashempour and T. L. Lee, "Integrated power factor correction and voltage fluctuation mitigation of microgrid using STATCOM," *2017 IEEE 3rd Int. Futur. Energy Electron. Conf. ECCE Asia, IFEEC - ECCE Asia 2017*, no. 3, pp. 1215–1219, 2017, doi: 10.1109/IFEEC.2017.7992215.

[6] Y. Jiang, J. Sun, W. Hu, S. Li, H. Zhou, and X. Zha, "Analysis and suppression of interaction between STATCOM and voltage-source inverter in islanded micro-grid," *2015 IEEE Energy Convers. Congr. Expo. ECCE 2015*, pp. 6858–6863, 2015, doi: 10.1109/ECCE.2015.7310620.

[7] A. A. Z. Diab, T. Ebraheem, R. Aljendy, H. M. Sultan, and Z. M. Ali, "Optimal design and control of MMC STATCOM for improving power quality indicators," *Appl. Sci.*, vol. 10, no. 7, 2020, doi: 10.3390/app10072490.

[8] H. Akagi, "Classification , Terminology , and Application of the Modular Multilevel Cascade Converter (MMCC)," no. Mmcc, pp. 508–515, 2010.

[9] a Lesnicar and R. Marquardt, "A new modular voltage source inverter topology," pp. 1–10, 2003.

[10] C. A. Bharadwaj, S. Maiti, and N. Dhal, "Control and State of Charge Balancing Technique of a Modular Multilevel STATCOM Integrated with Battery Energy Storage System," *2019 IEEE Students Conf. Eng. Syst. SCES 2019*, 2019, doi: 10.1109/SCES46477.2019.8977219.

[11] Q. Xiao *et al.*, "Modular multilevel converter based multi-terminal hybrid AC/DC microgrid with improved energy control method," *Appl. Energy*, vol. 282, no. PA, p. 116154, 2021, doi: 10.1016/j.apenergy.2020.116154.

[12] S. K. Chaudhary, A. F. Cupertino, R. Teodorescu, and J. R. Svensson, "Benchmarking of modular multilevel converter topologies for ES-STATCOM realization," *Energies*, vol. 13, no. 13, pp. 1–22, 2020, doi: 10.3390/en13133384.

[13] H. Bakir and A. A. Kulaksiz, "Modelling and voltage control of the solar-wind hybrid micro-grid with optimized STATCOM using GA and BFA," *Eng. Sci. Technol. an Int. J.*, vol. 23, no. 3, pp. 576–584, 2020, doi: 10.1016/j.jestch.2019.07.009.

[14] N. Quanminnzhu, *Modeling, Identification and Control Methods in Renewable Energy Systems*. in Green Energy and Technology. Singapore: Springer Singapore, 2019. doi: 10.1007/978-981-13-1945-7.

[15] N. Guler and E. Irmak, "MPPT based model predictive control of grid connected inverter for PV systems," *8th Int. Conf. Renew. Energy Res. Appl. ICRERA 2019*, pp. 982–986, 2019, doi: 10.1109/ICRERA47325.2019.8997105.

[16] V. Parque, S. Miura, and T. Miyashita, "Dynamic Response of a Wind Farm Consisting of Doubly-Fed Induction Generators to Network Disturbance," *Adv. Intell. Syst. Comput.*, vol. 873, pp. 222–238, 2019, doi: 10.1007/978-3-642-34336-0.

[17] Y. Lei, A. Mullane, G. Lightbody, and R. Yacamini, "Modeling of the wind turbine with a doubly fed induction generator for grid integration studies," *IEEE Trans. Energy Convers.*, vol. 21, no. 1, pp. 257–264, 2006, doi: 10.1109/TEC.2005.847958.

[18] A. M. Kassem, K. M. Hasaneen, and A. M. Yousef, "Dynamic modeling and robust power control of DFIG driven by wind turbine at infinite grid," *Int. J. Electr. Power Energy Syst.*, vol. 44, no. 1, pp. 375–382, 2013, doi: 10.1016/j.ijepes.2011.06.038.

[19] B. Saber, B. Abdelkader, B. Said, and B. Mansour, "Integral sliding mode control of four-leg DSTATCOM coupled with SMES unit," in *2017 5th International Conference on Electrical Engineering - Boumerdes, ICEE-B 2017*, 2017, pp. 1–6. doi: 10.1109/ICEE-B.2017.8192037.

[20] Y. Xu, Z. Y. Dong, and K. P. Wong, *Static Compensators (STATCOMs) in Power Systems*, vol. 90. in Power Systems, vol. 90. Singapore: Springer Singapore, 2015. doi: 10.1007/978-981-287-281-4.

[21] L. E. Christian, L. M. Putranto, and S. P. Hadi, "Design of Microgrid with Distribution Static Synchronous Compensator (D-STATCOM) for Regulating the Voltage Fluctuation," *Proc. 2019 7th Int. Conf. Smart Energy Grid Eng. SEGE 2019*, pp. 48–52, 2019, doi: 10.1109/SEGE.2019.8859860.

[22] B. Imtiaz, I. Zafar, and C. Yuanhui, "Modelling of an Optimized Microgrid Model by Integrating DG Distributed Generation Sources to IEEE 13 Bus System," *Eur. J. Electr. Eng. Comput. Sci.*, vol. 5, no. 2, pp. 18–25, 2021, doi: 10.24018/ejece.2021.5.2.309.

[23] P. V. Kapoor and M. M. Renge, "Comparative analysis of modular multilevel converter with different modulation technique for control of induction motor drive," *Microsyst. Technol.*, vol. 24, no. 8, pp. 3349–3356, 2018, doi: 10.1007/s00542-017-3692-2.